Photoacoustic tomography of water in phantoms and tissue

Zhun Xu
Changhui Li
Lihong V. Wang
Washington University
Department of Biomedical Engineering
Optical Imaging Laboratory
St Louis, Missouri 63130-4899

Abstract. Photoacoustic tomography (PAT) has been widely used to image optically absorptive objects in both human and animal tissues. For the first time, we present imaging of water with laser-based PAT. We photoacoustically measure the absorption spectra of water-ethanol mixtures at various water concentrations, and then image water-ethanol and pure-water inclusions in gel and a water inclusion in fat tissue. The significant difference in photoacoustic signals between water and fat tissue indicates that the laser-based PAT has the potential to detect water content in tissue. © *2010 Society of Photo-Optical Instrumentation Engineers.* [DOI: 10.1117/1.3443793]

Keywords: photoacoustic tomography; absorption spectroscopy; water content in tissue.

1 Introduction

The concentration of water in tissue reflects both physiological and pathological properties. Many techniques have been used to detect and measure water content in tissue. For instance, magnetic resonance imaging (MRI) was traditionally used to image water content in the brain,[1,2] bone,[3,4] and other tissues,[5,6] and diffusion-weight MRI (DW-MRI) has been used to map water mobility in brain and muscle tissues.[7,8] Recently, diffuse optical methods have been applied to measure the increased water concentration in tumors.[9] The bound water fraction, which is generally associated with tissue pathophysiology,[10] affects the molecular vibrational states of water. Diffuse optical spectroscopy (DOS) can measure the spectral changes due to bound water.[11] Although DOS is accurate and sensitive to water state,[11] its spatial location is poor.

As an emerging imaging technique, photoacoustic tomography (PAT) has been successfully implemented in biomedicine.[12–15] Combining high optical contrast and ultrasonic detection, PAT overcomes the depth limitation of other high-resolution optical imaging methods, and it is also free from speckle artifacts.[16–18]

PAT has been implemented to image various tissues[19] from centimeter-large breast tumors to micrometer-large single red blood cells. Image contrast has been provided by many endogenous and exogenous optical absorbers, such as hemoglobin, melanoma, and various natural and artificial contrast agents. Since water absorbs electromagnetic (EM) waves in the radio frequency (rf) and microwave spectra, it has served as the absorber in rf-based photoacoustic (PA) detection, which is also referred to as thermoacoustic (TA) detection. In addition, the absorption spectrum of water has a peak absorption coefficient of 0.45 cm^{-1} around 975 nm, with a FWHM of 920 to 1040 nm (Ref. 20). However, to our knowledge, water has never been detected by the PA imaging using a near-IR (NIR) light source. In this paper, we explore the potential of laser-based PA detection of water. From here on, the EM source is always a laser, unless otherwise noted.

The next section briefly introduces the theoretical basis. Then, we describe how the absorption spectra of water-ethanol mixtures at various concentrations were measured by using the PA technique. After that, both phantom and tissue experiments to image water are detailed. Finally, conclusions and a discussion are provided.

2 Theoretical Basis

The generation and propagation of a PA pressure wave in an acoustically homogenous and nonviscid infinite medium can be described as[21,22]

$$\left(\nabla^2 - \frac{1}{v_s^2}\frac{\partial^2}{\partial t^2}\right)p(\mathbf{r},t) = -\frac{\beta}{C_p}\frac{\partial}{\partial t}H(\mathbf{r},t), \qquad (1)$$

where $p(\mathbf{r},t)$ denotes the acoustic pressure at position $\mathbf{r}$ and time t, v_s is the speed of sound in the medium, β denotes the thermal coefficient of volume expansion, C_p denotes the isobaric specific heat capacity, and $H(\mathbf{r},t)$ is the heating function defined as the thermal energy converted at $\mathbf{r}$ and t per unit volume and time. For optical absorption, the heating function generally equals $\eta_{th}\mu_a\Phi(\mathbf{r},t)$, where η_{th} is the percentage of energy that is converted into heat, μ_a is the optical absorption coefficient, and Φ is the optical fluence rate.

In general, the initial pressure rise p_0 at $\mathbf{r}$ immediately after illumination by a short laser pulse is given by[23]

$$p_0(\mathbf{r}) = \Gamma(\mathbf{r})\eta_{th}\mu_a(\mathbf{r})F(\mathbf{r}), \qquad (2)$$

where $\Gamma = (\beta v_s^2)/C_p$ is defined as the Grueneisen coefficient (dimensionless), and F is the optical fluence. In many cases,

Address all correspondence to: Lihong V. Wang, Optical Imaging Laboratory, Department of Biomedical Engineering, Washington University, St. Louis, MO 63130-4899. Tel: 314-935-6152; Fax: 314-935-7448; E-mail: lhwang@biomed.wustl.edu
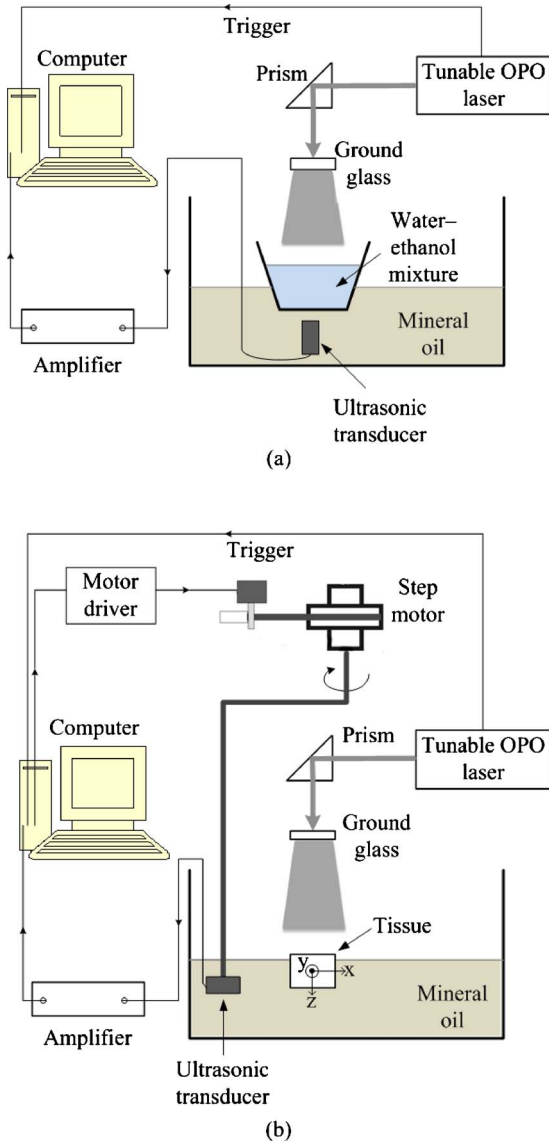
(a)

(b)

Fig. 1 Experimental setup of (a) water-ethanol mixture spectrum measurement and (b) phantom and tissue experiment.

η_{th} is approximately equal to 1. The initial pressure $p_0(\mathbf{r})$, serving as the source of the propagating PA pressure wave, depends on not only the illumination fluence and absorption coefficient, but also on the Grueneisen coefficient. In addition, the absorption coefficient is generally spectrally dependent.

3 Experimental and Theoretical Methods

Figure 1(a) shows the experimental setup of our absorption spectrum measurement system. The laser source was a tunable laser [Vibrant (HE) 355 I, OPOTEK], which provided laser pulses at a repetition rate of 10 Hz with a wavelength-tuning range of 925 to 1025 nm. Water-ethanol mixtures with the same volume in a thin-walled plastic container were placed in front of a 2.25-MHz unfocused ultrasonic transducer (V323, Panametrics), which was immersed in a tank of mineral oil.[24] The distance from the bottom surface of the mixture to the front surface of the transducer was ∼2 cm. Since the detected

signal amplitude is proportional to the initial pressure, here we used the peak-to-peak PA signal value to represent $p_0(\mathbf{r})$. The signal from the transducer was amplified by 40 dB by a pulse amplifier (5072 PR, Panametrics) and then recorded by a data acquisition card (CompuScope 14100, GaGe, Lockport, Illinois) at a sampling rate of 50 MHz. Both the mixture and the container generated PA signals, but the discontinuity at their interface helped to clearly distinguish between the two signals according to their different arrival times.

Six mixtures of water-ethanol with different volume concentrations of water were made: 100 (pure deionized water), 80, 60, 40, 20, and 0% (ethanol only). Since the ethanol used was 95% pure (Pharmco-Aaper, 190 proof) with the remaining 5% being water, the actual volume concentrations of water were 100, 81, 62, 43, 24, and 5%, respectively. The total volume of each mixture was set to 15 ml. PA measurement can quantify the relative initial pressure as a function of the optical wavelength at each of these concentrations. We calibrated the power of the laser in the spectral range from 925 to 1025 nm at 25-nm intervals. The laser pulse energy was recorded by a powermeter (Melles Griot broadband power/energy meter 13PEM001), and 20 laser pulses were averaged at each wavelength.

We calculated dependence of the Grueneisen coefficient on the mixture composition. The speed of sound v_s in the water-ethanol mixtures with different water concentrations were obtained from Ref. 25. The thermal coefficient of volume expansion β and specific heat capacity C_p of deionized water and pure ethanol were taken from Ref. 26. It was assumed that the thermal coefficient of volume expansion is additive with volume. That is, $\beta_m = (V_w/V_w + V_e)\beta_w + (V_e/V_w + V_e)\beta_e$, where V_w and V_e denote the volumes of water and ethanol, respectively; β_m is the thermal coefficient of the mixture; and β_w and β_e are the thermal coefficients of water and ethanol, respectively. We further assumed that C_p is also additive with mass. So $C_p^m = m_w C_p^w + m_e C_p^e$, where m_w and m_e denote the mass concentrations of water and ethanol, respectively. The mass could be calculated with the volume and density shown in Ref. 27. The specific heat capacities of the mixture, water, and ethanol are C_p^m, C_p^w, and C_p^e, respectively. Then, the Grueneisen coefficient of the mixture was calculated using $\Gamma = (\beta v_s^2)/C_p$.

Figure 1(b) shows the experimental setup of our PAT system, which was used to image water at various concentrations on the basis of the dependence of the PA signal on the water concentration. The tunable laser operated at the 975-nm wavelength. A 10-mJ pulse energy was used to excite PA signals. An ultrasound transducer (842-300, GE) with a center frequency of 2.25 MHz was immersed in the mineral oil in the tank. A step motor controlled by a computer drove the transducer to scan around the phantom through 120 positions evenly distributed along the horizontal scanning trajectory, while the PA signals were detected by the transducer. The same amplifier and data acquisition card shown in Fig. 1(a) were used. The image reconstruction was implemented in the computer after data acquisition using the image reconstruction algorithm described in Ref. 28.

Two samples were imaged using this PAT system. For sample 1, a gel cylinder made of an agar-water mixture[29] (4% agar) with three cylindrical holes was used. The diameter of
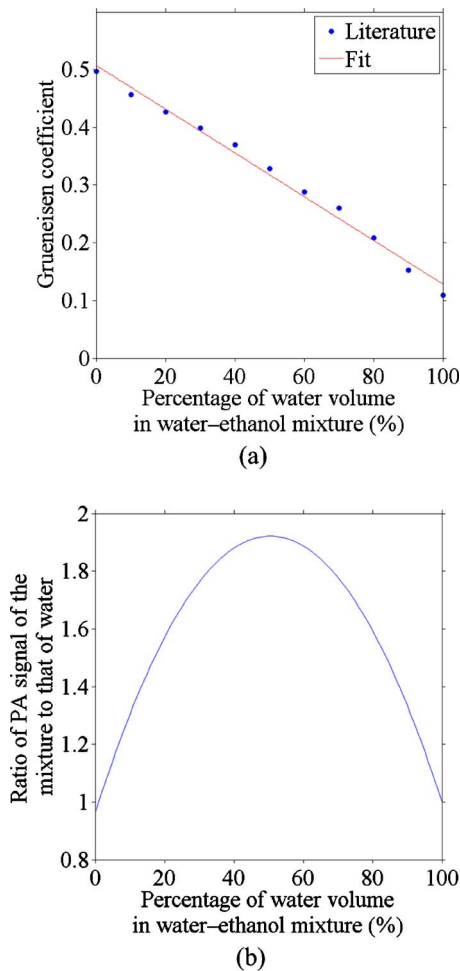
(a)

(b)

Fig. 2 (a) Grueneisen coefficient calculated based on the specific capacity, thermal volume expansion, and speed of sound data, a linear data fitting was also done ($R^2 = 0.99$); (b) relative PA signal of ethanol-water mixture as a function of water percentage (975 nm).

Fig. 3 Optical absorption coefficients from (a) PA (five means, for each mean, 100 PA signals were used) and (b) spectrophotometric measurements. Note that the 5% water solution is actually the ethanol stock solution. (c) Relative errors of the PA measurements from the spectrophotometric measurements at various wavelengths.

each hole was 5 mm. One hole was filled with deionized water, another with a 40% ethanol and 60% deionized water mixture, and the third hole was left in air [Fig. 5(a) in Sec. 4]. For sample 2, a piece of porcine fat was used. A hole was drilled in the fat and filled with 2% agar gel [Fig. 6(a) in Sec. 4].

4 Experimental Results

4.1 Spectral Measurement of Water-Ethanol Mixtures

From Eq. (2) in Sec. 2, the PA signal is in proportion to the absorption coefficient at a given Grueneisen coefficient. Thus, we can use PA signals to obtain the absorption spectra when Γ and F are known.

Figure 2(a) shows the estimated Grueneisen coefficients at various water concentrations of the mixtures. A line, fitted with the coefficient of simple determination $R^2 = 0.99$, was used to provide the Grueneisen coefficient values in estimating the optical absorption coefficient of each mixture.

By assuming that the absorption coefficient is additive on the water concentration and using the linear fit of the Grueneisen coefficient, we can get a quadratic dependence of the
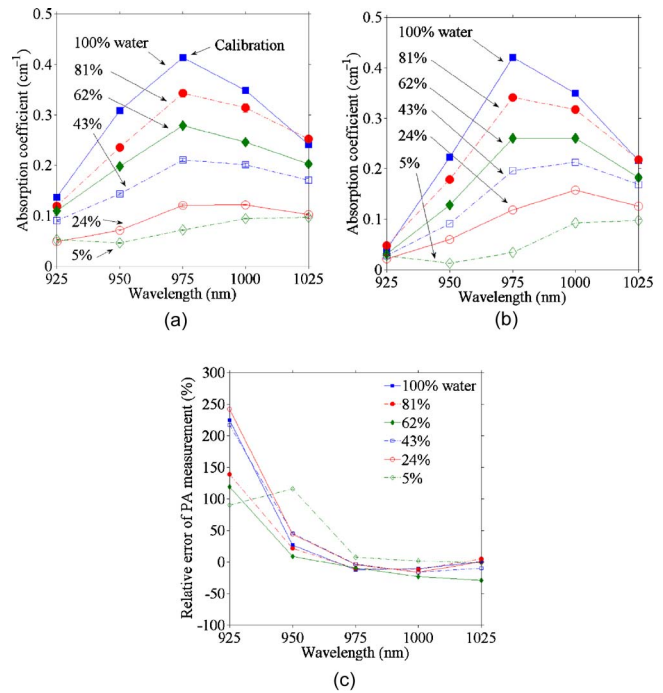
PA signal on the water concentration, as seen in Fig. 2(b). The figure plots the normalized PA signal to that of the pure deionized water. This quadratic relation is spectrally independent. The nonmonotonic curve in Fig. 2(b) implies that the water fraction of a water-ethanol mixture might not be determined uniquely according to the PA measurement alone. In general, one PA signal corresponds to two possible water concentrations. We measured relative PA signals at the 975-nm wavelength for five mixtures, and estimated the water concentration in Table 1. For the mixture with 50% water concentration, the ratio of its PA signal to that of the deionized water is greater than the maximum in the curve shown in Fig. 2(b). As a result, the solutions for the water concentration from multiple PA measurements were complex with a constant real part but a varying imaginary part. Only the real part is used as the photoacoustically measured water concentration, which matches the concentration for the peak of the curve in Fig. 2(b).

The relative absorption spectra were computed with Eq. (2) and then converted to absolute values [Fig. 3(a)] by calibrating with the absorption coefficient of deionized water at 975 nm measured by a spectrophotometer (Cary 5E, Varian, Walnut Greek, California). For Eq. (2), we used the Grueneisen coefficient shown in Fig. 2(a) and the calibrated optical fluence; the latter is assumed to be uniformly distributed owing to the ground glass shown in Fig. 1(a). For comparison, the absorption spectra were also measured with the spectrophotometer [Fig. 3(b)]. The relative errors between the PA and spectrophotometric data are plotted in Fig. 3(c), which shows good accordance except at 925 nm, where the absorption co-

Table 1 Comparison of water concentrations with corresponding PA-derived fractional values (five means; for each mean, 100 PA signals were used).

Preset water concentration	10%	30%	50%	70%	90%
Photoacoustically measured water concentration (solution 1)	8.5±0.4%	30.3±1.1%	50.6%	72.2±0.8%	89.0±0.5%
Photoacoustically measured water concentration (solution 2)	92.7±0.4%	70.9±1.1%	50.6%	28.9±0.8%	12.1±0.5%

efficient is small. In addition, the PA estimations for mixtures with less water were less accurate, possibly because of the inaccuracy in estimating the Grueneisen coefficient.

Because ethanol has negligible absorption in comparison to water at the spectral region of interest and the absorption coefficient is the product of the absorption cross section and the number density of the absorbers,[30] the absorption coefficient of each mixture is proportional to the water fraction. Therefore, we can use the absorption coefficients of deionized water and the ethanol stock solution (5% water) derived from the PA measurement to estimate the absorption coefficient of the known ratio of water and ethanol. The estimates and the PA experimental results are plotted in Fig. 4(a), and the relative errors are shown in Fig. 4(b). We can see that the estimations were accurate, especially at the wavelength of 975 nm and at high water concentrations, where the absorption coefficient was relatively large. Yet the estimation for the 24%
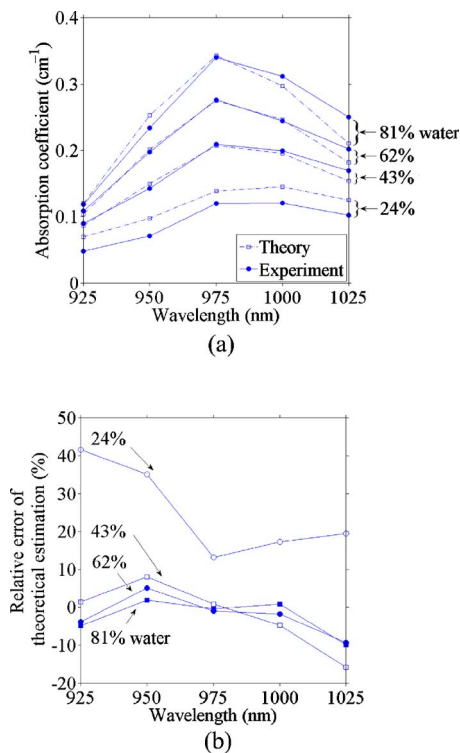
water concentration was less accurate (12.5% error at the 975-nm wavelength) than that for other mixtures (less than 5% error at the 975-nm wavelength).

4.2 Imaging Water Content in Phantoms and Tissue

Figure 5 shows a PAT image of objects with different water concentrations at 975 nm. The negative value is partially due to the limited bandwidth of the ultrasonic detection system. The reconstructed signal was integrated within the square marked in Fig. 5(b). The 40% water to 60% ethanol mixture yielded a higher PA signal than deionized water; about 1.65 times as great, which agrees with the ratio of 1.84 predicted from Fig. 2(b).

The tissue experiment [Fig. 6(b)] indicated that water generates nine times stronger PA signals than fat at the 975-nm wavelength [Fig. 6(c)]. This difference is possibly due to differences in both the absorption coefficient and the Grueneisen coefficient between water and fat. Thus, PAT has a great potential to detect localized water in fat.

5 Conclusions

We applied an NIR laser-based PA technique for the first time to image water. Absorption spectral measurements demonstrated that we could distinguish water signals of various concentrations. A tissue experiment showed the potential of water imaging *in vivo*. Different from previous applications in medi-
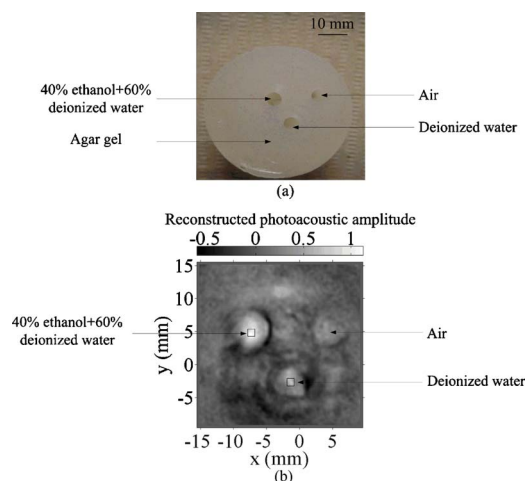

(a)

(b)

Fig. 4 (a) Comparison of theoretically calculated and photoacoustically measured absorption coefficient versus the optical wavelength and (b) relative error of the theoretically calculated absorption coefficient from the photoacoustically measured absorption coefficient versus the optical wavelength.

(a)

(b)

Fig. 5 Phantom experiment. (a) Photograph of a 4% agar gel with embedded objects of different water concentrations and (b) 2-D PA image of the phantom. Squares: areas for signal integration and comparison.
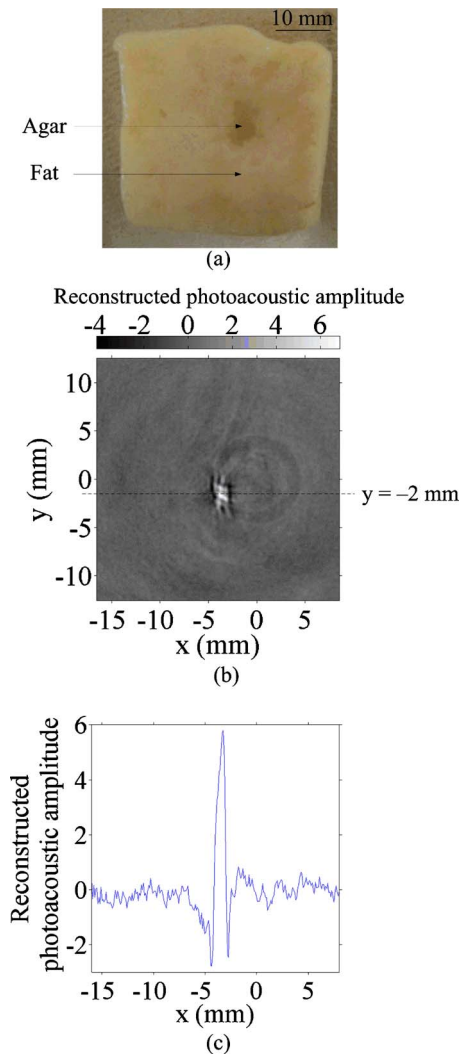
Fig. 6 Tissue experiment. (a) Photograph of fat tissue with an embedded 2% agar object, (b) 2-D PA image of the fat tissue, and (c) 1-D PA signal along $y=-2$ mm.

cal imaging, water imaging reflects not only the absorption coefficients but also the Grueneisen coefficients. In other words, different water concentrations lead to differences in both the optical absorption coefficient and the Grueneisen coefficient. PAT can image the differences in water content, especially in tissue with low water concentration such as fat, although the impact of absorption of skin and blood should be considered in animal experiments in the future.

Acknowledgments

References

1. D. J. Brooks, P. Luthert, D. Gadian, and C. D. Marsden, "Does signal-attenuation on high-field T2-weighted MRI of the brain reflect regional cerebral iron deposition—observations on the relationship between regional cerebral water proton T2 values and iron levels," *J. Neurol., Neurosurg. Psychiatry* **52**(1), 108–111 (1989).
2. R. Kreis, T. Ernst, and B. D. Ross, "Development of the human brain—in-vivo quantification of metabolite and water-content with proton magnetic-resonance spectroscopy," *Magn. Reson. Med.* **30**(4), 424–437 (1993).
3. P. Fantazzini, R. Viola, S. M. Alnaimi, and J. H. Strange, "Combined MR-relaxation and MR-cryoporometry in the study of bone microstructure," *Magn. Reson. Imaging* **19**(3–4), 481–484 (2001).
4. X. D. Wang and Q. W. Ni, "Determination of cortical bone porosity and pore size distribution using a low field pulsed NMR approach," *J. Orthop. Res.* **21**(2), 312–319 (2003).
5. R. Mathurdevre, "Biomedical implications of the relaxation behavior of water related to NMR imaging," *Br. J. Radiol.* **57**(683), 955–976 (1984).
6. F. Mirrashed and J. C. Sharp, "*In vivo* morphological characterisation of skin by MRI micro-imaging methods," *Skin Res. Technol.* **10**(3), 149–160 (2004).
7. P. J. Basser, J. Mattiello, and D. Lebihan, "MR diffusion tensor spectroscopy and imaging," *Biophys. J.* **66**(1), 259–267 (1994).
8. J. V. Hajnal, M. Doran, A. S. Hall, A. G. Collins, A. Oatridge, J. M. Pennock, I. R. Young, and G. M. Bydder, "MR imaging of anisotropically restricted diffusion of water in the nervous-system—technical, anatomic, and pathological considerations," *J. Comput. Assist. Tomogr.* **15**(1), 1–18 (1991).
9. A. Cerussi, N. Shah, D. Hsiang, A. Durkin, J. Butler, and B. J. Tromberg, "*In vivo* absorption, scattering, and physiologic properties of 58 malignant breast tumors determined by broadband diffuse optical spectroscopy," *J. Biomed. Opt.* **11**(4), 044005 (2006).
10. J. B. Brubach, A. Mermet, A. Filabozzi, A. Gerschel, and P. Roy, "Signatures of the hydrogen bonding in the infrared bands of water," *J. Chem. Phys.* **122**(18), 184509 (2005).
11. S. H. Chung, A. E. Cerussi, C. Klifa, H. M. Baek, O. Birgul, G. Gulsen, S. I. Merritt, D. Hsiang, and B. J. Tromberg, "*In vivo* water state measurements in breast cancer using broadband diffuse optical spectroscopy," *Phys. Med. Biol.* **53**(23), 6713–6727 (2008).
12. R. A. Kruger, "Photoacoustic ultrasound," *Med. Phys.* **21**(1), 127–131 (1994).
13. A. A. Karabutov, N. B. Podymova, and V. S. Letokhov, "Time-resolved laser optoacoustic tomography of inhomogeneous media," *Appl. Phys. B: Lasers Opt.* **63**(6), 545–563 (1996).
14. A. A. Oraevsky, S. L. Jacques, and F. K. Tittel, "Measurement of tissue optical properties by time-resolved detection of laser-induced transient stress," *Appl. Opt.* **36**(1), 402–415 (1997).
15. L. H. V. Wang, X. M. Zhao, H. T. Sun, and G. Ku, "Microwave-induced acoustic imaging of biological tissues," *Rev. Sci. Instrum.* **70**(9), 3744–3748 (1999).
16. X. D. Wang, Y. J. Pang, G. Ku, X. Y. Xie, G. Stoica, and L. H. V. Wang, "Noninvasive laser-induced photoacoustic tomography for structural and functional *in vivo* imaging of the brain," *Nat. Biotechnol.* **21**(7), 803–806 (2003).
17. C. H. Li and L. H. V. Wang, "Photoacoustic tomography and sensing in biomedicine," *Phys. Med. Biol.* **54**(19), R59–R97 (2009).
18. L. V. Wang, "Multiscale photoacoustic microscopy and computed tomography," *Nat. Photonics* **3**(9), 503–509 (2009).
19. L. H. V. Wang, "Prospects of photoacoustic tomography," *Med. Phys.* **35**(12), 5758–5767 (2008).
20. G. M. Hale and M. R. Querry, "Optical constants of water in the 200 nm to 200 μm wavelength region," *Appl. Opt.* **12**, 555–563 (1973).
21. P. M. Morse and K. U. Ingard, *Theoretical Acoustics*, McGraw-Hill, New York (1968).
22. G. J. Diebold, T. Sun, and M. I. Khan, "Photoacoustic monopole radiation in 1-dimension, 2-dimension, and 3-dimension," *Phys. Rev. Lett.* **67**(24), 3384–3387 (1991).
23. L. V. Wang, "Tutorial on photoacoustic microscopy and computed tomography," *IEEE J. Sel. Top. Quantum Electron.* **14**(1), 171–179 (2008).
24. M. Pramanik, M. Swierczewska, D. Green, B. Sitharaman, and L. V. Wang, "Single-walled carbon nanotubes as a multimodal-thermoacoustic and photoacoustic-contrast agent," *J. Biomed. Opt.* **14**(3), 034018 (2009).
25. H. Hobæk, Ã. Voll, R. Fardal, and L. Calise, "Experiment on finite amplitude sound propagation in a fluid with a strong sound speed

gradient," *AIP Conf. Proc.* **838**(1), 593–600 (2006).

26. H. D. Young, R. M. Geller, and F. W. Sears, *Sears & Zemansky's College Physics*, Pearson/Addison Wesley, San Francisco (2007).

27. B. Gonzalez, N. Calvar, E. Gomez, and A. Dominguez, "Density, dynamic viscosity, and derived properties of binary mixtures of methanol or ethanol with water, ethyl acetate, and methyl acetate at $T = (293.15, 298.15, \text{ and } 303.15)$ K," *J. Chem. Thermodyn.* **39**(12), 1578–1588 (2007).

28. C. H. Li and L. H. V. Wang, "Photoacoustic tomography of the mouse cerebral cortex with a high-numerical-aperture-based virtual point detector," *J. Biomed. Opt.* **14**(2), 024047 (2009).

29. C. Kim, A. Garcia-Uribe, S.-R. Kothapalli, and L. V. Wang, "Optical phantoms for ultrasound-modulated optical tomography," in *Design and Performance Validation of Phantoms Used in Conjunction with Optical Measurements of Tissue*, *Proc. SPIE* **6870**, 68700M (2008).

30. L. V. Wang and H.-I. Wu, *Biomedical Optics: Principles and Imaging*, Wiley, New York (2007).